Engineering 7 (2021) 515–525

Contents lists available at ScienceDirect

Engineering

journal homepage: www.elsevier.com/locate/eng

Research
Clean Energy—Article

Effect of Radial Porosity Oscillation on the Thermal Performance of Packed Bed Latent Heat Storage

H. B. Liu, C. Y. Zhao *

Institute of Engineering Thermo-Physics, School of Mechanical Engineering, Shanghai Jiao Tong University, Shanghai 200240, China

ARTICLE INFO

Article history:
Received 4 December 2019
Revised 1 May 2020
Accepted 5 May 2020
Available online 22 September 2020

Keywords:
Packed bed latent heat storage
Radial porosity oscillation
Fluid flow
Heat transfer
Diameter ratio

ABSTRACT

Owing to its high heat storage capacity and fast heat transfer rate, packed bed latent heat storage (LHS) is considered as a promising method to store thermal energy. In a packed bed, the wall effect can impact the packing arrangement of phase change material (PCM) capsules, inducing radial porosity oscillation. In this study, an actual-arrangement-based three-dimensional packed bed LHS model was built to consider the radial porosity oscillation. Its fluid flow and heat transfer were analyzed. With different cylindrical sub-surfaces intercepted along the radial direction in the packed bed, the corresponding relationships between the arrangement of capsules and porosity oscillation were identified. The oscillating distribution of radial porosity led to a non-uniform distribution of heat transfer fluid (HTF) velocity. As a result, radial temperature distributions and liquid fraction distributions of PCMs were further affected. The effects of different dimensionless parameters (e.g., tube-to-capsule diameter ratio, Reynolds number, and Stefan number) on the radial characteristics of HTF and PCMs were discussed. The results showed that different diameter ratios correspond to different radial porosity distributions. Further, with an increase in diameter ratio, HTF velocity varies significantly in the near wall region while the non-uniformity of HTF velocity in the center region will decrease. The Reynolds and Stefan numbers slightly impact the relative velocity distribution of the HTF—while higher Reynolds numbers can lead to a proportional improvement of velocity, an increase in Stefan number can promote heat storage of the packed bed LHS system.

1. Introduction

Recently, solar energy has been extensively used for its advantages of cleanness, safety, and inexhaustibility [1,2]. According to REN21, the capacity of a solar photovoltaic (PV) and concentrating solar power (CSP) was up-regulated from 409.9 GW in 2017 to 510.5 GW in 2018, occupying 60.97% of the renewable energy growth [3]. However, solar energy is intermittent and fluctuating, and requires energy storage technology to address its defects and improve energy efficiency. Considering the thermal utilization of solar energy, latent heat storage (LHS) can exhibit a higher energy density and maintain an almost constant temperature during phase change, which brought widespread attention [4,5]. The main constraint of LHS is the low thermal conductivity of phase change materials (PCMs) (0.2–0.8 $W \cdot m^{-1} \cdot K^{-1}$), and requires effective heat transfer enhancements [6]. Considering the heat storage unit, a packed bed is considered an efficient approach when compared with a shell-and-tube unit. As reported by Li et al. [7], the charging and discharging rates of a packed bed LHS system is 1.8–3.2 times that of the shell-and-tube heat storage system.

In the packed bed LHS system, as an heat transfer fluid (HTF) directly flows through the PCM capsules, the arrangement of PCM capsules considerably impacts the flow field [8,9]. For a sphere packing, the densest arrangements of the spheres include hexagonal packing and face-centered cubic packing, exhibiting a highest packing density as 74.05% [10]. However, when spheres are randomly packed in a container, they cannot be densely arranged because of the wall, which is called the wall effect [11]. Mueller [12] reported that radial porosity would oscillate along the radial direction in the packed bed. Moreover, the oscillation distribution of radial porosity causes non-uniformity of the flow filed, which would further affect the heat transfer inside the packed bed [13]. Considering a cylindrical container, the wall effect on the average packing density is prominent with a decrease in diameter ratio of the container and spheres (D/d_p) [14]. When a packed bed is used for latent heat storage, higher heat storage

* Corresponding author.
E-mail address: changying.zhao@sjtu.edu.cn (C.Y. Zhao).

https://doi.org/10.1016/j.eng.2020.05.020
2095-8099/

capacity leads to smaller tank size and diameter ratio. Accordingly, the radial porosity variation should be considered in a numerical study on packed bed LHS systems, particularly for small diameter ratio (D/d_p < 10) [15].

Several numerical models were built to assess the thermal performance of the packed bed LHS system. Based on the requirement for the specific arrangement of PCM capsules, the models can be divided into representative elementary volume (REV) scale model and pore scale model. In REV scale model, governing equations are adopted to calculate the thermal performance of HTF and PCM. Benmansour et al. [16] adopted the two-phase model to express the energy equations of HTF and PCMs, while the porosity employed in the equations is a constant; thus, the radial porosity variation was not considered [17]. Subsequently, a monotonic exponential equation, where the porosity refers to a function of radial distance from the wall, was proposed to replace the constant porosity [18,19]. To obtain the thermal gradients inside the PCM capsules, the dispersion-concentric (DC) model was proposed. Karthikeyan and Velraj [20] compared the two-phase model with the DC model; they reported that the results of the DC model complied better with their experimental results as the internal heat transfer inside the PCM capsules was considered. However, a packed bed with a small diameter ratio (D/d_p < 10) cannot be considered as a continuous porous medium. Since representative control volume should be small enough to gain good calculation results, a control volume would not contain even more than one capsule, which fails to satisfy the requirement of the REV scale model [21,22].

In the pore scale model, the concrete arrangement of PCM capsules should be described; subsequently, the flow of HTF and the heat transfer between HTF and PCM capsules can be calculated. Xia et al. [23] developed an effective packed model, where the three-dimensional (3D) packed bed is converted to a two-dimensional packed bed. The corresponding criteria was to ensure that the two packed beds exhibit identical porosity. However, the radial porosity distribution is not considered during the transformation. Moreover, PCM capsules in the effective model are not in contact with each other, leading to the change of flow channels among PCM capsules. Therefore, the flow field is not accurate and heat conduction between capsules is ignored.

Thus, complying with the actual packing process of spheres, a 3D packed bed LHS model was built to consider the radial porosity oscillation. The mechanism of the radial porosity oscillation and its impacts on the radial velocity of HTF, and radial temperature and liquid fraction of PCMs are analyzed. Further, the effects of different dimensionless parameters (e.g., diameter ratio, Reynolds number, and Stefan number) on the fluid flow, heat transfer, and heat storage performance of the packed bed LHS are discussed.

2. Model description

2.1. Establishment of physical model

In studying a 3D packed bed, a difficulty faced is building an effective sphere packing model; the falling, collision, and friction process of the spheres should be simulated. The existing methods of building a packed bed consist of the discrete equation method (DEM) method [8,24,25], Blender method [26,27], and Monte Carlo method [15,28]. In this study, the open source software Blender was adopted to build a 3D packed bed model. The Blender software was equipped with a prominent physical simulator and bullet physics library; thus, the physical process of spheres when they fall under the influence of gravity can be effectively calculated. In the modelling process, a cylindrical container was first built; then, small spheres were constantly and randomly generated to fall above the container, as illustrated in Fig. 1(a). The position of every sphere was calculated during the packing process. If the positions of all the spheres are stable, the packing process can be considered to be attaining a steady state. Then, the 3D packed bed model is established.

Porosity (φ_v) is the ratio of void volume (V_{void}) to total volume (V), while surface porosity (φ_A) is the ratio of void area (A_{void}) to total area (A) on surface, as expressed in Eqs. (1)–(3) [29].

$$\varphi_v = \frac{V_{void}}{V} \tag{1}$$

$$\varphi_A = \frac{A_{void}}{A} \tag{2}$$

$$\varphi_v = \frac{\int_0^R \varphi_A(r) \cdot 2\pi r dr}{\pi R^2} \tag{3}$$

where R is the radius of container and r is an independent variable changing from 0 to R. Radial porosity, which is discussed in this study, is a phenomenon of surface porosity. To calculate the radial porosity, a series of cylindrical sub-surfaces along the radial direction were cut off. For the corresponding sub-surface, a ray-casting algorithm was adopted to determine the areas pertaining to the interior of the spheres. Then, the areas of all the spheres are added and total area of spheres is divided by the area of the sub-surface, as presented in Fig. 1(b).

In Fig. 2, the radial porosity of the model built in the Blender was compared with the results of the Mueller, and the corresponding diameter ratio obtained is 7.99 [12]. The two curves oscillate

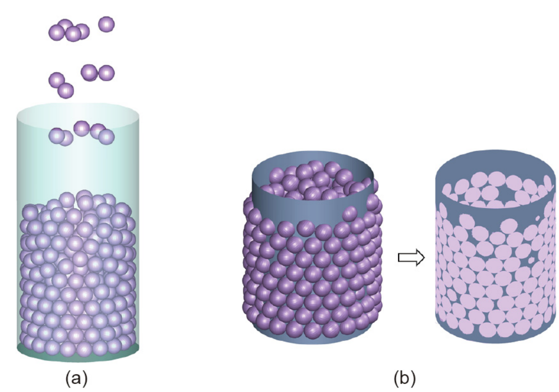

Fig 1. Schematic diagrams of (a) packing process of sphere and (b) generation of sub-surfaces along the radial direction.

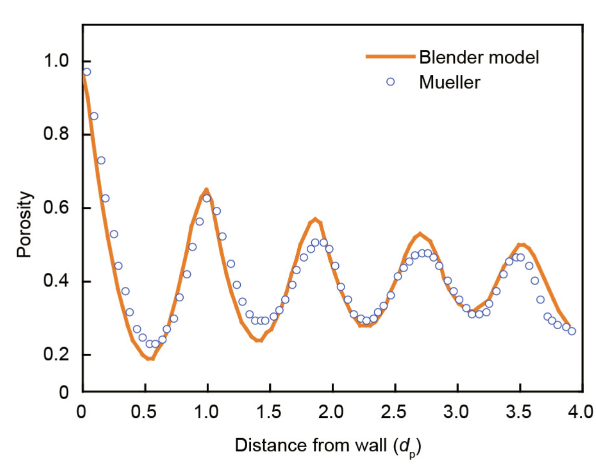

Fig 2. Comparison of radial porosity distributions when diameter ratio is 7.99.

and correspond well with each other, verifying the reliability of the model. Moreover, the oscillation distribution of radial porosity shows that the packed bed cannot be treated as a uniform porous media, further confirming the necessity of establishing a 3D model.

In the packed bed, the contact type between the spheres is point contact, which is not conducive to the mesh generation. Thus, four methods were proposed to address contact points: overlaps, gaps, caps, and bridges. The bridge method can achieve the optimal results in the situation of heat transfer [30]. Accordingly, small cylinders with a diameter of $d_p/10$ were inserted between every two spheres in contact as heat bridges, thereby leading to changes in the average porosity of the packed bed by 0.05%–0.08%. Moreover, the gaps method was used to address the contact points between the spheres and container wall. After the diameter of the container was increased by 1 mm, a narrow gap was identified between the spheres and container wall.

Further, a 3D packed bed LHS model was built, as presented in Fig. 3. In the model, 205 PCM capsules were packed into a cylindrical tank with an inner diameter of 240 mm, and the diameter of PCM capsule is 48 mm; thus, the diameter ratio of the packed bed is 5. Ternary carbonate Li_2CO_3–K_2CO_3–Na_2CO_3 (32 wt%–35 wt%–33 wt%) was selected as the PCM, and its thermal properties are listed in Table 1. The packed bed was placed in the middle section, while extended parts were added on the sides of the inlet and outlet to eliminate the impact of the sides.

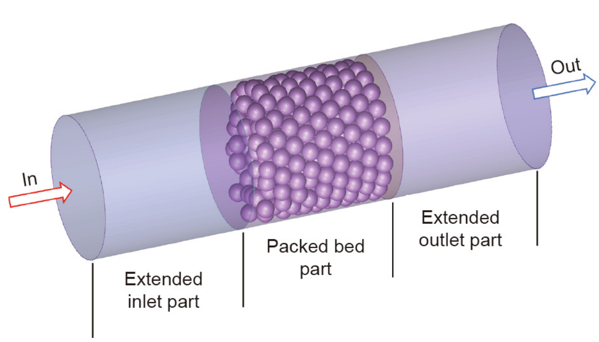

Fig. 3. Schematic diagram of 3D packed bed LHS system.

2.2. Mathematical model

2.2.1. Assumptions

(1) The effect of gravity on HTF flow is ignored;

(2) The convection effect of the PCM in the capsules is ignored;

(3) Radiation heat transfer of the HTF and PCM capsules is ignored.

2.2.2. Governing equation of HTF

In the packed bed LHS system, the pore Reynolds number based on mean velocity is expressed as [9]

$$Re_p = \frac{\rho(u_{in}/\varphi_v)d_p}{\mu} \tag{4}$$

where ρ is density, μ is viscosity, and u_{in} is the inlet velocity.

For a packed bed with low diameter ratio, the flow is normally turbulent flow. Considering that the heat transfer surface of the PCM capsule is spherical, renormalization group (RNG) k–ε turbulence model was selected to facilitate the wall treatment. Subsequently, the governing equations of the HTF in the packed bed LHS system can be written as follows [31]:

Continuity equation:

$$\frac{\partial \rho}{\partial t} + \frac{\partial(\rho u_i)}{\partial x_i} = 0 \tag{5}$$

Momentum equation:

$$\frac{\partial}{\partial t}(\rho u_i) + \frac{\partial}{\partial x_j}(\rho u_i u_j) = -\frac{\partial p}{\partial x_i} + \frac{\partial}{\partial x_j}\left[\mu\left(\frac{\partial u_i}{\partial x_j} + \frac{\partial u_j}{\partial x_i} - \frac{2}{3}\delta_{ij}\frac{\partial u_i}{\partial x_j}\right) - \left(\overline{\rho u_i' u_j'}\right)\right] \tag{6}$$

Energy equation:

$$\frac{\partial}{\partial t}(\rho E) + \frac{\partial}{\partial x_i}(\rho u_i E) = \frac{\partial}{\partial x_i}\left[\left(\lambda + \frac{c_p \mu_t}{\sigma_T}\right)\frac{\partial T}{\partial x_j} + u_i(\tau_{ij})_{eff}\right] \tag{7}$$

k equation:

$$\frac{\partial}{\partial t}(\rho k) + \frac{\partial}{\partial x_i}(\rho k u_i) = \frac{\partial}{\partial x_j}\left[\left(\mu + \frac{\mu_t}{\sigma_k}\right)\frac{\partial k}{\partial x_j}\right] + G_k - \rho\varepsilon \tag{8}$$

ε equation:

$$\frac{\partial}{\partial t}(\rho \varepsilon) + \frac{\partial}{\partial x_i}(\rho \varepsilon u_i) = \frac{\partial}{\partial x_j}\left[\left(\mu + \frac{\mu_t}{\sigma_\varepsilon}\right)\frac{\partial \varepsilon}{\partial x_j}\right] + C_{1\varepsilon}\frac{\varepsilon}{k}G_k - C_{2\varepsilon}\rho\frac{\varepsilon^2}{k} - R_\varepsilon \tag{9}$$

where, x_i and x_j are the distance in i and j directions, respectively; u_i and u_j are the velocity of HTF in i and j directions, respectively; u_i' and u_j' are the fluctuating velocity of HTF in i and j directions, respectively; δ_{ij} is the Kronecker delta; E is the energy; $(\tau_{ij})_{eff}$ is the effective Reynolds-stress tensor; k is the turbulent kinetic energy; ε is the turbulence dissipation rate; σ_T is the Prandtl number in energy equation; σ_k is the Prandtl number in turbulent kinetic energy equation; σ_ε is the Prandtl number in turbulence dissipation rate equation; C_1 and C_2 are two model constants. The turbulent viscosity μ_t, generation of turbulence kinetic energy G_k, and additional term R_ε are expressed as [32]

$$\mu_t = \rho C_\mu \frac{k^2}{\varepsilon} \tag{10}$$

$$G_k = \mu_t\left(\frac{\partial u_i}{\partial x_j} + \frac{\partial u_j}{\partial x_i}\right)\frac{\partial u_j}{\partial x_i} \tag{11}$$

$$R_\varepsilon = \frac{C_\mu \rho \gamma^3 (1 - \gamma/\gamma_0)}{1 + 0.012\gamma^3}\cdot\frac{\varepsilon^2}{0.012} \tag{12}$$

$$\gamma = Sk/\varepsilon,\ S = \sqrt{2S_{ij}S_{ij}},\ S_{ij} = \frac{1}{2}\left(\frac{\partial u_i}{\partial x_j} + \frac{\partial u_j}{\partial x_i}\right) \tag{13}$$

where C_μ is the model constant; γ is the RNG k–ε turbulence model coefficient; γ_0 is the RNG k–ε turbulence model coefficient in the initial state; S denotes the mean strain-rate of the flow; and S_{ij} is the deformation tensor.

Table 1
Thermal properties of PCM.

PCM	T_s (°C)	T_l (°C)	ΔH (kJ·kg^{-1})	λ (W·m^{-1}·K^{-1})	c_p (J·kg^{-1}·K^{-1})	ρ (kg·m^{-3})
Li_2CO_3–K_2CO_3–Na_2CO_3	395.1	413.0	273.0	1.69 (s); 1.60 (l)	1540 (s); 1640 (l)	2310

T_s: solid state temperature; T_l: liquid state temperature; ΔH: specific enthalpy; λ: thermal conductivity; c_p: specific heat capacity; ρ: density; s: solid state; l: liquid state.

The constants in the aforementioned equations are σ_T = 1.0, σ_k = σ= 0.72, C_μ= 0.0845, C_1= 1.42, C_2 = 1.68, and γ_0 = 4.38.

2.2.3. Governing equation of the PCMs in the capsules

For the PCMs in the capsules, as the internal natural convection is ignored, the energy equation can be expressed as [23]

$$\frac{\partial}{\partial t}\left(\rho_{\mathrm{pcm}} H_{\mathrm{pcm}}\right) - \nabla \cdot \left(\lambda_{\mathrm{pcm}} \nabla T_{\mathrm{pcm}}\right) = 0 \tag{14}$$

where H_{pcm} is the enthalpy of PCM and defined as the sum of sensible heat and latent heat; ∇ is the gradient operator.

$$H_{\mathrm{pcm}} = H_{0,\mathrm{pcm}} + \int_{T_0}^{T_{\mathrm{pcm}}} c_{\mathrm{p,pcm}} \mathrm{d}T_{\mathrm{pcm}} + \Delta H \tag{15}$$

where $H_{0,\mathrm{pcm}}$ is the enthalpy of the PCM at the initial temperature. ΔH represents the latent heat released during the charging process and defined as $\Delta H = \beta L$. L is the latent heat and β is the liquid fraction of PCM, which, at different temperatures, is written as follows:

$$\beta = 0, \text{ while } T_{\mathrm{pcm}} < T_{\mathrm{s}} \tag{16}$$

$$\beta = 1, \text{ while } T_{\mathrm{pcm}} > T_{\mathrm{l}} \tag{17}$$

$$\beta = \frac{T_{\mathrm{pcm}} - T_{\mathrm{s}}}{T_{\mathrm{l}} - T_{\mathrm{s}}}, \text{ while } T_{\mathrm{s}} \le T_{\mathrm{pcm}} \le T_{\mathrm{l}} \tag{18}$$

where T_{pcm}, T_0, T_{s}, and T_{l} denote the temperature of the PCM, initial temperature, onset melting temperature, and ending melting temperature, respectively. Furthermore, the charging process of the PCM demonstrates a ratio of sensible heat to latent heat, which is defined as the Stefan number [33]:

$$\mathrm{Ste} = \frac{c_{\mathrm{p,pcm}}(T_{\mathrm{in}} - T_{\mathrm{l}})}{L} \tag{19}$$

where T_{in} refers to the temperature of the inlet HTF.

2.2.4. Boundary conditions and initial conditions

At the initial state, the packed bed LHS system was maintained at a constant temperature and heat transfer fluid temperature $T_{\mathrm{f}} = T_{\mathrm{pcm}} = T_0$. During the charging process, the HTF at the inlet was maintained at a constant temperature and mass flow rate (q), while heat flux of the HTF in the direction normal to the outlet was assumed to be zero. Therefore, the boundary conditions of the HTF in the packed bed are expressed as follows:

$$T_{\mathrm{f}} = T_{\mathrm{in}},\ q_{\mathrm{f}} = q_{\mathrm{in}}, \text{ at the inlet} \tag{20}$$

$$\partial T_{\mathrm{f}}/\partial z = 0, \text{ at the outlet} \tag{21}$$

where z is the height.

To understand the effect of radial porosity distribution on the radial characteristics of the HTF, the container wall is set to be adiabatic.

$$\partial T_{\mathrm{wall}}/\partial r|_R = 0 \tag{22}$$

2.3. Heat storage of packed bed LHS system

The total heat storage in the packed bed LHS system consists of the heat stored in the PCM, PCM capsule shells, and heat stored in the tank wall. The heat stored in the PCM includes the sensible heat in the solid and liquid state, and latent heat during phase change. The heat stored in the PCM capsule shells and tank refers to the sensible heat. The charging time of the system is defined as the time when the central temperature of the PCM capsule at the outlet reaches 1 K lower than the inlet temperature. Hence, the total heat storage (Q_{total}) in the packed bed LHS system can be expressed as follows:

$$Q_{\mathrm{total}} = Q_{\mathrm{pcm}} + Q_{\mathrm{shell}} + Q_{\mathrm{tank}} \tag{23}$$

$$Q_{\mathrm{pcm}} = m_{\mathrm{pcm}}\left[c_{\mathrm{p,s}}(T_{\mathrm{m}} - T_0) + \Delta H + c_{\mathrm{p,l}}(T_{\mathrm{in}} - T_{\mathrm{m}})\right] \tag{24}$$

$$Q_{\mathrm{shell}} = m_{\mathrm{shell}} c_{\mathrm{p,shell}}(T_{\mathrm{in}} - T_0) \tag{25}$$

$$Q_{\mathrm{tank}} = m_{\mathrm{tank}} c_{\mathrm{p,tank}}(T_{\mathrm{in}} - T_0) \tag{26}$$

where Q_{pcm}, Q_{shell}, and Q_{tank} are the heat storage in the PCM, shell of PCM capsules, and the tank, respectively; m_{pcm}, m_{shell}, and m_{tank} are the quality of PCM, shell of PCM capsules, and the tank, respectively; $c_{\mathrm{p,s}}$ and $c_{\mathrm{p,l}}$ are the specific heat capacity of the PCM in solid state and liquid state, respectively; T_{m}, T_0, and T_{in} are the melting temperature, the initial temperature, and the inlet temperature, respectively; $c_{\mathrm{p,shell}}$ and $c_{\mathrm{p,tank}}$ are the heat capacity of the shell and tank, respectively.

During the charging process, heat storage of the packed bed LHS system (Q_{stored}) can be obtained using the first law of thermodynamics:

$$Q_{\mathrm{stored}} = \int \dot{m}_{\mathrm{f}}\left(c_{\mathrm{pf,in}} T_{\mathrm{f,in}} - c_{\mathrm{pf,out}} T_{\mathrm{f,out}}\right)\mathrm{d}T \tag{27}$$

where m_{f} is the mass flow rate of HTF; $c_{\mathrm{pf,in}}$ and $c_{\mathrm{pf,out}}$ are the specific heat capacity of HTF at the inlet and outlet, respectively; $T_{\mathrm{f,in}}$ and $T_{\mathrm{f,out}}$ are the temperature of HTF at the inlet and outlet, respectively.

The average charging power P_{aver} can be defined as [7]

$$P_{\mathrm{aver}} = \frac{Q_{\mathrm{stored}}}{\tau_{\mathrm{charge}}} \tag{28}$$

where τ_{charge} is the charging time.

2.4. Numerical procedure and validation

As there are hundreds of PCM capsules randomly filled in the packed bed, unstructured grids were adopted to generate the meshes. The shrink-wrap method was employed to generate the surface mesh, and then, the volume was filled with the polyhedral meshes [34]. Subsequently, the effects of grid size on the charging time and pressure drop in the packed bed were determined, and a grid size of $d_{\mathrm{p}}/18$ was selected for the mesh generation, as shown in Fig. 4. During the calculation, pressure and velocity fields were computed using the SIMPLE algorithms. The spatial discretization and transient formulation were calculated using the second order upwind scheme and second order implicit scheme, respectively.

Li et al. [7] built a packed bed LHS system filled with 385 PCM capsules. The inner diameter of the container was 260 mm, while the capsule diameter was 34 mm; thus, a diameter ratio of 7.65

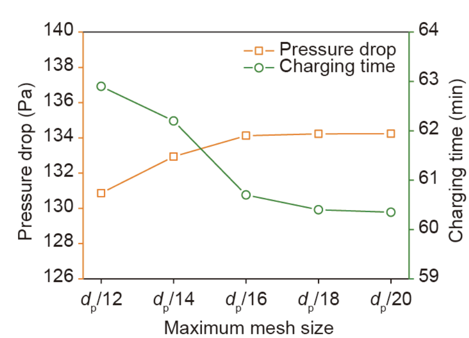

Fig. 4. Independence verification of mesh size.

was achieved. The PCM in the capsules was ternary carbonate Li_2CO_3–K_2CO_3–Na_2CO_3 (32 wt%–35 wt%–33 wt%); its thermal properties are listed in Table 1. The PCM temperature variations at different heights during the charging process were selected to verify the established 3D packed bed LHS model. The locations of the PCM capsules along the height were z/h = 0.25, 0.5, 0.75, as shown in Fig. 5(a). During the charging process, the mass flow rate q_{in} was 260 kg·h^{-1}, while the initial temperature T_0 of the packed bed was 325 °C and inlet temperature T_{in} of the HTF reached 465 °C.

As shown in Fig. 5(b), the simulation data of the model complied well with the experimental results, and the results at z/H = 0.5 were optimally matched. At the beginning of the charging process, the simulation was faster than the experiment, whereas, after the phase change process of the PCM capsule was achieved, the simulation data and experimental results were synchronized. On one hand, the heating process of the HTF to be heated from initial temperature (e.g. 325 °C) to the inlet temperature (e.g. 465 °C) was time-consuming, whereas, this transformation was attained immediately in the simulation. On the other hand, when the PCMs were in the liquid phase, the differences of the heat storage attributed to the different inlet temperature transition mode will be small when compared with the overall heat storage of the system. Accordingly, the simulation becomes more accurate over time. The 3D packed bed LHS system model exhibits a good accuracy.

3. Results and discussion

3.1. Flow and thermal performance analysis

In this part, the initial temperature T_0 of the packed bed is 325 °C, inlet temperature T_{in} of HTF is 465 °C, and mass flow rate reaches 260 kg·h^{-1}. As the average porosity is 0.437 in the packed bed exhibiting the diameter ratio of 5, the Reynolds number Re_p is calculated to be 4998.72, thus confirming that the flow in the packed bed is turbulent.

3.1.1. Reason for radial porosity oscillation

For the packed bed LHS system model with a diameter ratio of 5, the distribution of the radial porosity is illustrated in Fig. 6. Several cylindrical sub-surfaces at different radial positions inside the packed bed were intercepted. The distance of the sub-surfaces from the tank wall reaches 0, 0.25d_p, 0.5d_p, 0.75d_p, d_p, 1.25d_p, 1.5d_p, 1.75d_p, and 2d_p, respectively. Considering the surface porosity, the porosity of the sub-surfaces (0, d_p, and 2d_p away from the wall) is suggested to be higher than that of the other sub-surfaces. The oscillating distribution of the radial porosity is related to the process of packing capsules and spherical shape of the capsules. During the packing process, capsules tend to fill the space close to the wall first and subsequently fill the space in the center [35]. At the wall surface, the PCM capsules exhibit point contacts with the tank wall. Hence, the porosity of this position is close to 1, indicating that the sub-surface is almost HTF. At the position 0.5d_p away from the wall, the sub-surface passes through the center of the capsules, revealing that the PCM area will occupy most of the area of the sub-surface, and the porosity will decrease to 0.15. Similarly, at the sub-surface d_p away from the wall, the capsules near the wall are in point contacts with the inner capsules. Gaps are formed near the contact points, and the porosity increases with a value of 0.67. Thus, the porosity of the sub-surfaces in the radial direction complies with an oscillating distribution.

3.1.2. Flow velocity distribution

Similar to radial porosity, radial velocity is the average value of HTF velocity on the sub-surface, defined as Eq. (29). In this study, the relative velocity (U) is determined by the ratio of the radial velocity ($u(r)$) to the inlet velocity (u_{in}).

$$u(r) = \frac{1}{A_f} \iint_{\Omega_f} |u| \mathrm{d}A \tag{29}$$

$$U(r) = \frac{u(r)}{u_{in}} \tag{30}$$

where Ω_f is the area of HTF on the sub-surface and A_f is the area value of HTF. The relative velocity distribution of the HTF at different radial positions is presented in Fig. 7, also indicating an oscillation trend. It is observed that although the porosity at the wall is close to 1, the flow velocity is 0 due to wall viscosity. However, in the radial direction away from the wall, velocity increases significantly and subsequently varies with the oscillation of radial porosity. When the HTF ascends into the packed bed, it flows through the gaps among the PCM capsules. Locations with more gaps allow more HTF to flow through; thus, the HTF velocity is faster where the porosity is larger. To facilitate the analysis and comparison of the velocity distribution, the relative velocity distribution was divided into two parts: near wall region and center region. The distance of the near wall region varies from the wall to 0.5d_p, where velocity varies drastically, while the center region is from 0.5d_p to the center, and the velocity varies more regularly.

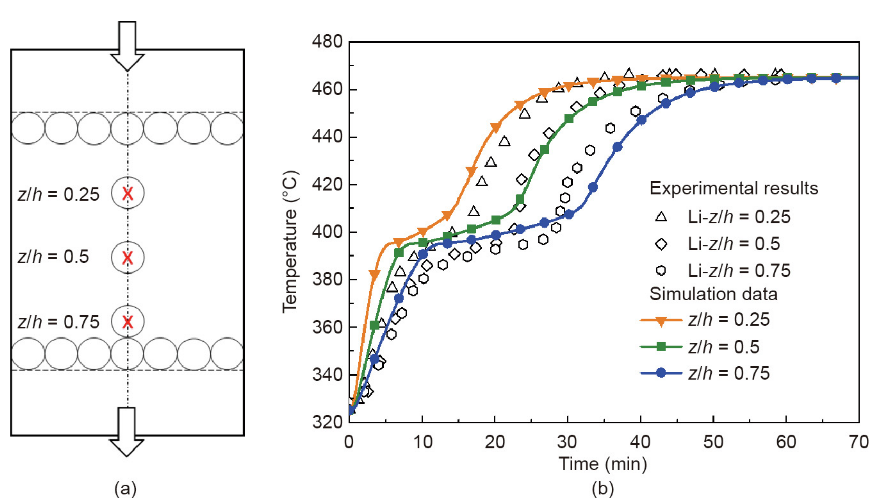

Fig. 5. (a) Position illustrations of thermocouples; (b) comparison of calculation results with experimental data.

In the near wall region, velocity varies drastically. Hence, the most important parameter here is the maximum relative velocity near the wall. In this case, the maximum relative velocity at the near wall region is 3.49. According to the continuity equation, under the same flow rate, the variation of velocity is inversely proportional to the variation of flow channel area, as expressed in Eq. (31). Accordingly, the velocity of the incompressible HTF increases with a sudden contraction of flow channel. Fig. 8 illustrates the velocity distributions on several cross-sections in the packed bed. The velocity increases in the area near the wall for the contraction of flow channel.

$$\frac{u_1}{u_0} = \frac{A_0}{A_1} \tag{31}$$

The relative velocity distribution in the center region exhibits a more regular oscillation that is consistent with the radial porosity distribution. To assess the non-uniformity of the HTF, the standard deviation of relative velocity was adopted. A higher standard deviation complies with a less uniform velocity distribution. For the packed bed with a diameter ratio of 5, when the Reynolds number Re_p is 4998.72, the standard deviation of the relative velocity (s_U) in the center region is 0.39.

$$s_U = \sqrt{\frac{1}{N}\sum_{i=1}^{N}\left(U_i - \bar{U}\right)^2} \tag{32}$$

where, N is the number of sub-surfaces, U_i is the relative velocity at the No. i sub-surface; $\bar{U}$ is the average relative velocity of all the sub-surfaces.

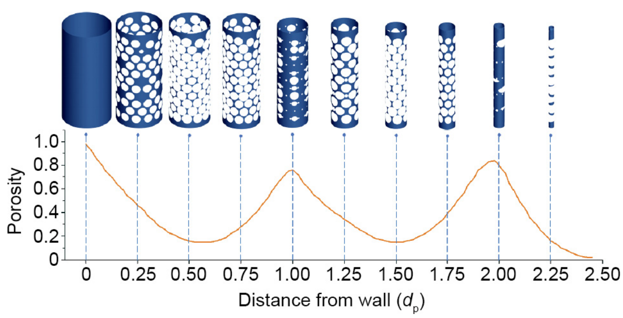

Fig. 6. Radial porosity distribution and sub-surfaces along the radial direction.

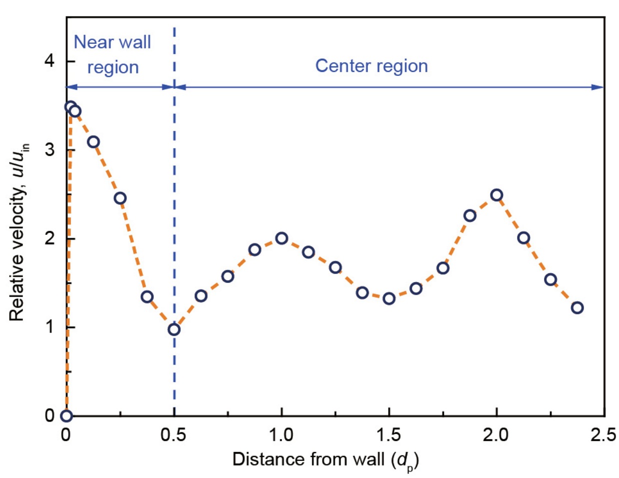

Fig. 7. Relative velocity distribution along the radial direction.

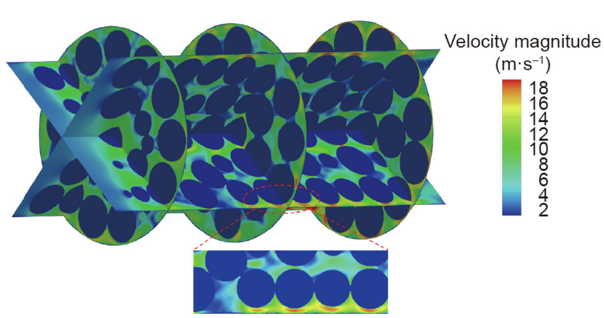

Fig. 8. Flow velocity distribution inside the packed bed.

3.1.3. Radial temperature and liquid fraction distribution

For the corresponding sub-surface, the radial temperature and liquid fraction of the PCMs are calculated as Eq. (33) and Eq. (34), where Ω_{pcm} is the area of the PCMs on the sub-surface and A_{pcm} is the area of the PCMs.

$$T(r) = \frac{1}{A_{pcm}} \iint_{\Omega_{pcm}} T\mathrm{d}A \tag{33}$$

$$\beta(r) = \frac{1}{A_{pcm}} \iint_{\Omega_{pcm}} \beta\mathrm{d}A \tag{34}$$

To illustrate the radial distribution variations of PCMs during the charging process, the temperature and liquid fraction of the PCMs on the sub-surfaces at different time are presented in Figs. 9(a) and (b), fluctuating along the radial direction. When

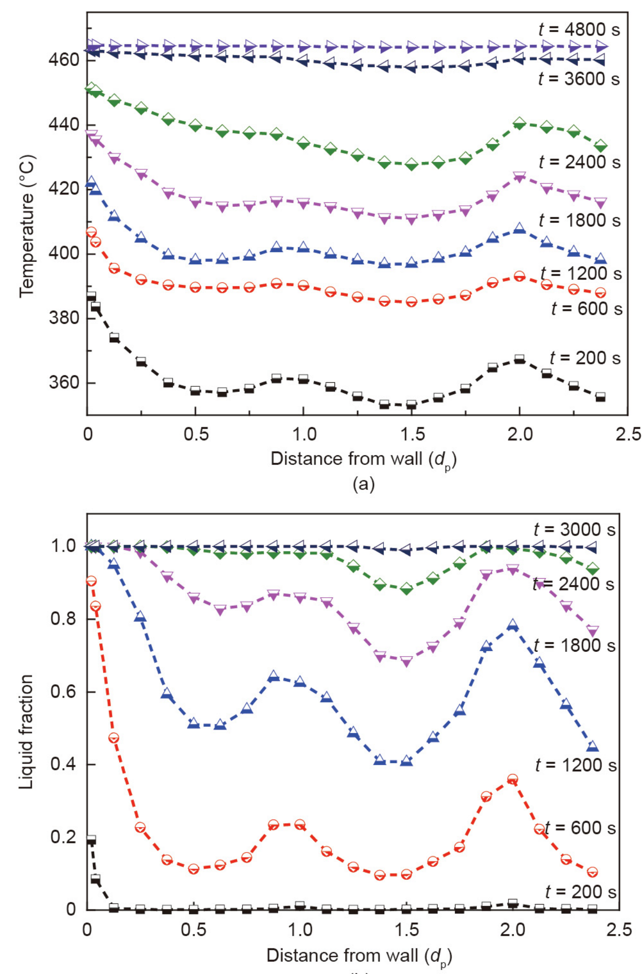

Fig. 9. Radial distributions of PCMs at different time. (a) Temperature; (b) liquid fraction.

t = 200 s, except for the near wall region, the PCMs' temperatures at most positions do not attain the melting point, and the liquid fractions remain 0. Thus, the charging process remains in the solid-state heating stage. When t = 1200 s, the PCMs' temperatures are within the melting temperature range, and the liquid fraction differs significantly at each position. The melting temperature range of PCM is 395.1–413 °C. Considering the enthalpy method, an increase temperature for every 1 °C leads to an elevation of the PCM liquid fraction by 0.056. Accordingly, although the temperature differences of the PCMs are small, the liquid fractions variations are high. When t = 2400 s, the PCMs' temperatures at most positions are greater than the final melting temperature, and the liquid fractions become 1 indicating that the charging process is in the liquid-state heating stage.

In Fig. 10, the liquid fractions of PCMs on the radial sub-surfaces are observed when t = 600 s. The PCMs near the entrance melt faster, and the melting is initiated from the flow side of the HTF. Moreover, the PCMs melt faster on the sub-surfaces of d_p and $2d_p$ away from the wall, complying with the liquid fraction distribution in Fig. 9(b). For the low porosity on the sub-surfaces, that is $0.5d_p$ and $1.5d_p$ away from the wall, the flow velocity is slow, while the convection heat transfer is weak. The proportions of the PCMs are higher on the sub-surfaces corresponding to $0.5d_p$ and $1.5d_p$ away from wall; thus, the amount of heat required for melting increases leading to a longer charging process.

3.2. Effect of diameter ratio on the flow and thermal performance

In this section, the effects of various diameter ratios (4, 5, 6) on the flow and thermal performance of the packed bed LHS system are studied; at the inlet temperature T_{in} of 465 °C, the mass flow rate is 260 kg·h^{-1}. The inner diameter of the heat storage tank is 240 mm, and the height is 500 mm. To determine the number of PCM capsules in each packed bed, the heat storage of the three packed bed LHS systems was set to be nearly equal. Based on the aforementioned criterion, the parameters of the three packed beds are listed in Table 2. In Fig. 11, the radial porosity distributions of the packed beds with different diameter ratios are compared, and it is observed that the radial porosity distributions oscillate but exhibit different trends. Over a distance of $1.5d_p$ from the wall, the radial porosity distributions are almost constant, whereas, as the distance gets closer to the center, more significant differences are observed. For the packed bed with a diameter ratio of 4, the diameter can be filled with 4 capsules, and the capsules are in point contacts or no contact at the tank center, in which gaps are formed. Consequently, the porosity is large. For the packed bed with a diameter ratio of 5, the diameter can be filled with 5 capsules; thus, the tank center is filled with the capsules, and the central porosity is approximately zero. For the packed bed with a diameter ratio of 6, the central porosity ought to be as large as that of the packed bed with a diameter ratio of 4, theoretically. However, as the tank center is slightly far away from the tank wall, and the wall effect decreases, the packing of capsules at the tank center tends to be random, as shown in Fig. 11.

The flow relative velocity distributions inside the three packed bed LHS systems are illustrated in Fig. 12(a). It is observed that the relative velocity distributions along the radial direction comply with the radial porosity distributions. At the near wall region, the maximum relative velocity increases with an increase in the diameter ratio, which is 2.87, 3.49, and 3.99, respectively. With a decrease in the diameter of the PCM capsule, gaps formed between the capsules and container wall are smaller. As shown in Eq. (31), when hot air flows through a narrower channel, the flow velocity will increase. For the center region, the standard deviation of relative velocity distribution in the three packed beds reaches 0.53, 0.39, and 0.27, respectively, thus demonstrating that an increase of diameter ratio can decrease the velocity non-uniformity in the center region.

The radial liquid fraction distributions of the packed beds when t = 1200 s are shown in Fig. 12(b). For the packed bed with a diameter ratio of 4, the PCMs near the wall and tank center melt faster than the other positions. However, for the packed bed with the diameter ratio of 5 and 6, the charging processes of PCMs near the wall are faster than those at the tank center, which is consistent with the radial porosity distributions.

In Fig. 13, the heat storage and average charging power of the packed bed LHS systems with different diameter ratios were calculated. With an increase in the diameter ratio, the charging times of the three systems are 121.03, 89.73, and 79.80 min, respectively; thus, the average charging powers of the packed bed LHS systems increase. The capsule diameter in the system with a diameter ratio of 4 is 60 mm, while that with the diameter ratio of 5 or 6 achieves

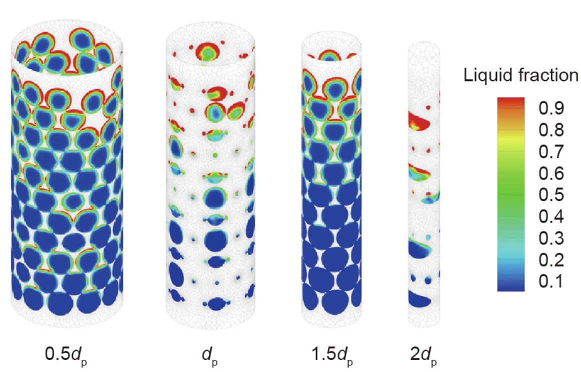

Fig. 10. Liquid fractions of PCMs on the radial sub-surfaces when t = 600 s.

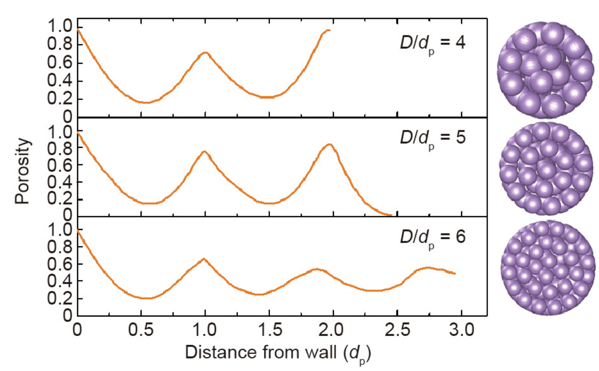

Fig. 11. Radial porosity distributions of the packed bed models with different diameter ratios.

Table 2
Parameters of the packed bed LHS systems with different diameter ratios.

Diameter ratio	Capsule diameter (mm)	Capsule number	Shell thickness (mm)	Average porosity
4	60	105	2	0.458
5	48	205	2	0.437
6	40	354	2	0.428

a diameter of 48 or 40 mm. A smaller diameter indicates a shorter heat transfer distance, whereas it will further result in a denser packing arrangement and promotes a decrease in pressure. The calculated results show that the decrease in pressure in the packed beds are 142.97, 213.34, and 257.13 Pa, respectively. Hence, higher pump power is required to maintain the operation of the packed bed LHS system. Accordingly, when the packed bed LHS system is employed for practical use, the charging time, charging power, and pressure drop should be comprehensively considered.

3.3. Effect of Reynolds number on the flow and thermal performance

Three different Reynolds numbers (4229.69, 4998.72, and 5767.75) are compared, which comply with inlet flow rates of 220, 260, and 300 kg·h^{-1}, respectively. The diameter ratio of packed bed is 5, and the Stefan number is 0.31. Fig. 14(a) shows that the relative velocities of the HTF along the radial direction for different Reynolds numbers comply with a similar distribution. The maximum relative velocities of the HTF at the near wall region are 3.40, 3.49, and 3.55, while the standard deviations of relative velocity at the center region are 0.40, 0.39, and 0.39, demonstrating

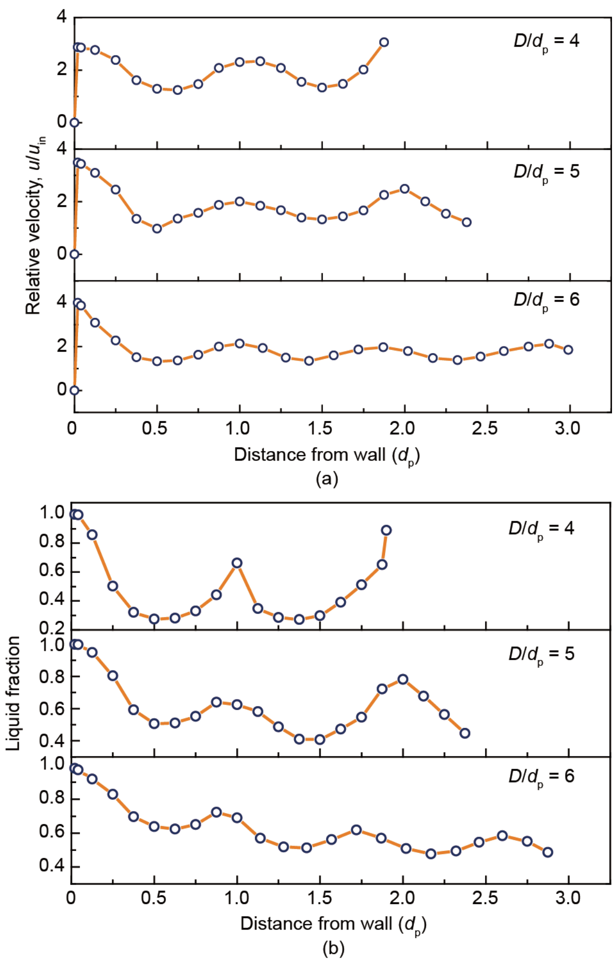

Fig. 12. Radial distributions of the packed bed LHS systems with different diameter ratios. (a) Relative velocity; (b) liquid fraction when t = 1200 s.

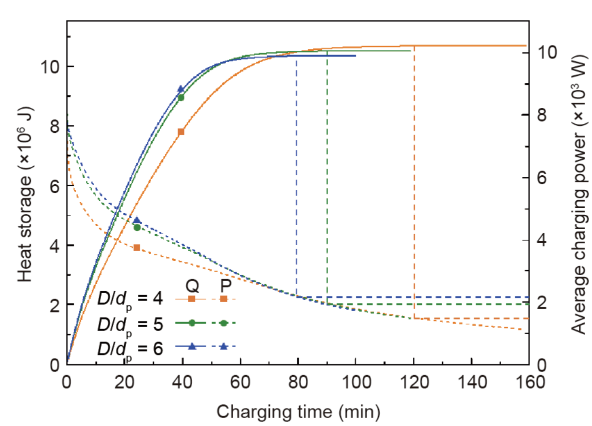

Fig. 13. Heat storage and the average charging power of the packed bed LHS systems with different diameter ratios.

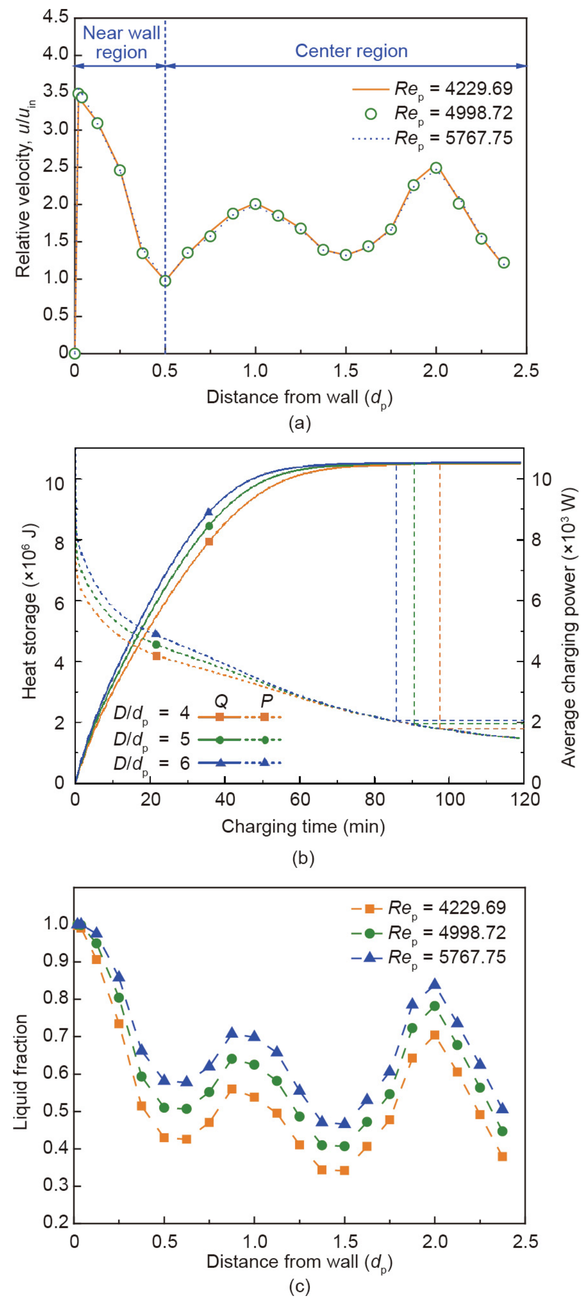

Fig. 14. Flow and thermal properties in the packed bed LHS systems with different Reynolds numbers. (a) Radial relative velocity distribution; (b) heat storage and the average charging power; (c) radial liquid fraction distribution when t = 1200 s.

that an increase in the Reynolds number would result in a proportional improvement in velocity. Correspondingly, convection heat transfer in the packed bed is enhanced, and the charging process of the PCMs would accelerate (Fig. 14(b)). The PCMs melt faster with an increase in the Reynolds number when t = 1200 s.

Fig. 14(c) shows that an increase in the Reynolds number will not promote heat storage of the system, while the charging time can be shortened and charging power can increase accordingly. The charging time of the system with Re_p = 4229.69 is 97.53 min, while those of the systems with Re_p = 4998.72 and Re_p = 5767.75 are 89.73 and 83.63 min, and 8% and 14.25% faster, respectively. However, an increase in the Reynolds number would increase the dissipation of the HTF when flowing through capsules and improve the pressure drop at the inlet and outlet. The corresponding pressure drops in the three conditions reach 162.84, 213.34, and 270.06 Pa, respectively.

3.4. Effect of Stefan number on the flow and thermal performance

Similar to the previous section, the diameter ratio of the packed bed is 5 and Reynolds number is 4998.72. Subsequently, the HTF inlet temperatures are set to 445, 465, and 485 °C, leading to Stefan numbers of 0.19, 0.31, and 0.43, respectively. A comparison of the relative velocity distributions is drawn in Fig. 15(a). It is observed that the increase in Stefan number slightly impacts the flow velocity and its radial distribution is almost constant. Hence, the convection effect between the HTF and PCM capsules is the same. However, an increase in the Stefan number can increase the temperature differences between the HTF and PCM capsules, which enhances the heat transfer to the PCMs. Thus, the charging processes of the PCMs is facilitated and PCMs melt faster, as presented in Fig. 15(b).

An increase in the Stefan number further indicates that the sensible heat stored in the PCMs increase, thus, the heat storage of the packed bed LHS system is improved (Fig. 15(c)). When the Stefan number is 0.19, the charging time is 99.2 min, and the charging time becomes 89.73 and 84.7 min with an increase in the Stefan number to 0.31 and 0.43, respectively. Accordingly, an increase in the Stefan number can shorten the charging time while increasing the heat storage and average charging power.

4. Conclusion

In this study, a 3D packed bed LHS model was built, where the radial porosity oscillation caused by the wall effect was considered. The model was validated by comparing the temperature variations of PCM capsules with the experimental results. The impact of the radial porosity oscillation on the radial velocity of HTF, radial temperature of PCMs, and liquid fraction of PCMs were studied. Moreover, the effects of different dimensionless parameters (e.g., diameter ratio, Reynolds number, and Stefan number) on the radial characteristics of the HTF and PCMs were discussed. The main conclusions are as follows:

(1) The oscillating distribution of the radial porosity is analyzed by intercepting different cylindrical sub-surfaces along the radial direction. For the sub-surface where the capsules are in point contact with the container wall or inner capsules, the gaps formed result in high porosity. However, for the sub-surfaces that pass through the capsules, the PCMs occupy most of the area on the surface, and a lower porosity is observed.

(2) The oscillating distribution of the radial porosity leads to a non-uniform distribution of the HTF velocity. The velocity would change sharply at the near wall region while an oscillating distribution at the center region is observed. The radial temperature distribution of the PCMs is consistent with the radial relative velocity distribution of the HTF. Hence, the PCMs melt faster at the radial positions with higher porosity.

(3) With an increase in the diameter ratio, the maximum velocity at the near wall region increases. However, as the packing of the PCM capsules in the center of the tank becomes more random, the velocity non-uniformity in the center region decreases. Furthermore, the charging time of the packed bed LHS system decreases drastically and average charging power can be improved, whereas larger pressure drops are observed.

(4) An increase in the Reynolds number would result in a proportional improvement of the velocity and accelerate the charging processes of the PCMs, which further shortens the charging time

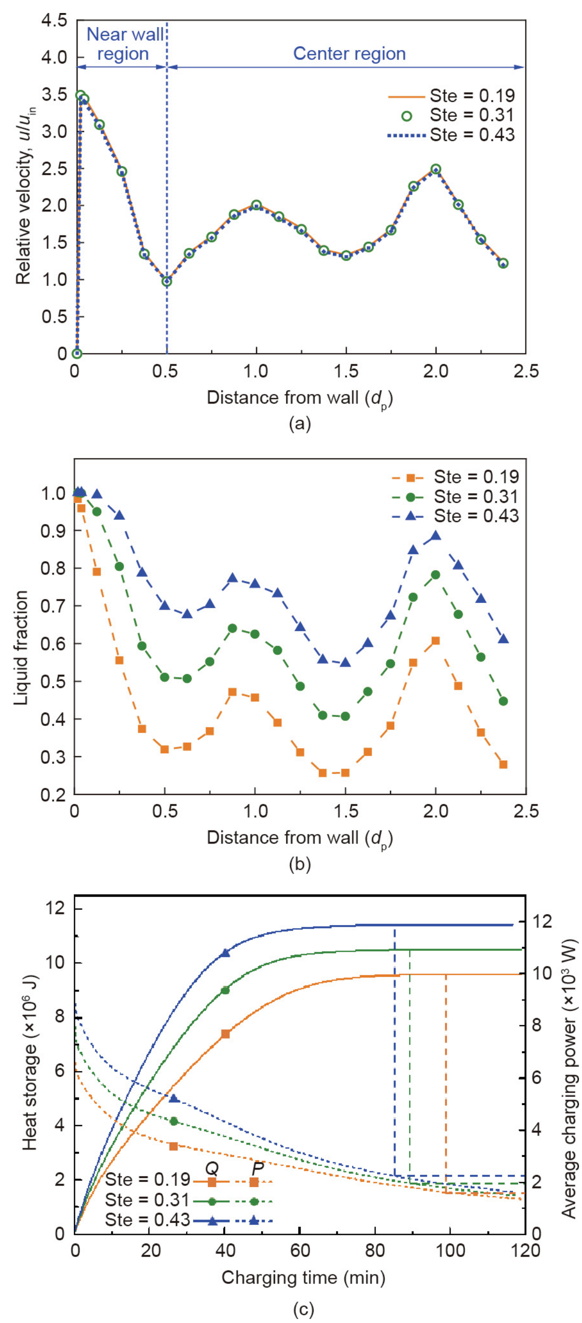

Fig. 15. Flow and thermal properties in the packed bed LHS systems with different Stefan numbers. (a) Radial relative velocity distribution; (b) radial liquid fraction distribution when t = 1200 s; (c) heat storage and the average charging power.

and increases the average charging power. This can cause larger pressure drops.

(5) An increase in the Stefan number slightly impacts the velocity distribution of the HTF, whereas it can enhance the temperature differences between the HTF and PCMs, and the sensible heat stored in PCMs. Thus, the charging time can be shortened and heat storage of the packed bed LHS system increases.

Acknowledgements

This work is supported by the Foundation for Innovative Research Groups of the National Natural Science Foundation of China (51521004) and the National Natural Science Foundation of China (51906150).

Compliance with ethics guidelines

H. B. Liu and C. Y. Zhao declare that they have no conflict of interest or financial conflicts to disclose.

Nomenclature

V	volume (m^3)
A	area (m^2)
d_p	diameter of PCM capsule (m)
R	radius of container (m)
D	diameter of container (m)
T	temperature (°C)
H	specific enthalpy ($kJ \cdot kg^{-1}$)
c_p	specific heat capacity ($J \cdot kg^{-1} \cdot K^{-1}$)
L	latent heat ($kJ \cdot kg^{-1}$)
E	energy (J)
Ste	Stefan number
q	mass flow rate ($kg \cdot s^{-1}$)
u	velocity ($m \cdot s^{-1}$)
u'	fluctuating velocity ($m \cdot s^{-1}$)
U	relative velocity
Re_p	pore Reynolds number
t	time (s)
x	distance (m)
z	height (m)
p	pressure (Pa)
k	turbulent kinetic energy ($m^2 \cdot s^{-2}$)
c_1, c_2	model constants in turbulent kinetic energy equation
c	model constant in turbulent viscosity correlation
Q	heat storage (J)
P	charging power (W)
s	standard deviation of relative velocity
φ	porosity
ρ	density ($kg \cdot m^{-3}$)
λ	thermal conductivity ($W \cdot m^{-1} \cdot K^{-1}$)
μ	viscosity ($kg \cdot m^{-1} \cdot s^{-1}$)
μ_t	turbulent viscosity ($kg \cdot m^{-1} \cdot s^{-1}$)
σ_T	Prandtl number in energy equation
σ_k	Prandtl number in turbulent kinetic energy equation
σ_ε	Prandtl number in turbulence dissipation rate equation
ε	turbulence dissipation rate ($m^2 \cdot s^{-3}$)
β	liquid fraction
γ	RNG k–ε turbulence model coefficient
Ω	area of HTF and PCM

Subscripts

i, j	coordinate direction
f	heat transfer fluid
PCM	phase change material
total	total amount
shell	shell of PCM capsule
tank	tank of container
stored	stored heat
charge	charging process
aver	average value
in	inlet
0	the initial state
l	liquid state
s	solid state

References

[1] Lewis NS. Research opportunities to advance solar energy utilization. Science 2016;351(6271):aad1920.

[2] Kabir E, Kumar P, Kumar S, Adelodun AA, Kim KH. Solar energy: potential and future prospects. Renew Sustain Energy Rev 2018;82:894–900.

[3] Ren21 [Internet]. Renewables 2019 global status report. Paris: REN21; 2019 [cited 2020 May 8]. Available from: http://www.ren21.net/gsr-2019/.

[4] Zhao Y, You Y, Liu HB, Zhao CY, Xu ZG. Experimental study on the thermodynamic performance of cascaded latent heat storage in the heat charging process. Energy 2018;157:690–706.

[5] Sciacovelli A, Gagliardi F, Verda V. Maximization of performance of a PCM latent heat storage system with innovative fins. Appl Energy 2015;137:707–15.

[6] Zhang HL, Baeyens J, Caceres G, Degreve J, Lv YQ. Thermal energy storage: recent developments and practical aspects. Pror Energy Combust Sci 2016;53:1–40.

[7] Li MJ, Jin B, Ma Z, Yuan F. Experimental and numerical study on the performance of a new high-temperature packed-bed thermal energy storage system with macroencapsulation of molten salt phase change material. Appl Energy 2018;221:1–15.

[8] Das S, Deen NG, Kuipers JAM. A DNS study of flow and heat transfer through slender fixed-bed reactors randomly packed with spherical particles. Chem Eng Sci 2017;160:1–19.

[9] Gunjal PR, Ranade VV, Chaudhari RV. Computational study of a single-phase flow in packed beds of spheres. AIChE J 2005;51(2):365–78.

[10] Mackay A. A dense non-crystallographic packing of equal spheres. Acta Crystallogr 1962;15(9):916–8.

[11] Mueller GE. Numerically packing spheres in cylinders. Powder Technol 2005;159(2):105–10.

[12] Mueller GE. Radial void fraction distributions in randomly packed fixed beds of uniformly sized spheres in cylindrical containers. Powder Technol 1992;72(3):269–75.

[13] Kamiuto K, Saitoh S. Fully developed forced-convection heat transfer in cylindrical packed beds with constant wall heat fluxes. JSME Int J Ser B Fluids Therm Eng 1996;39(2):395–401.

[14] McGeary RK. Mechanical packing of spherical particles. J Am Ceram Soc 1961;44(10):513–22.

[15] Freund H, Zeiser T, Huber F, Klemm E, Brenner G, Durst F, et al. Numerical simulations of single phase reacting flows in randomly packed fixed-bed reactors and experimental validation. Chem Eng Sci 2003;58(3–6):903–10.

[16] Benmansour A, Hamdan MA, Bengeuddach A. Experimental and numerical investigation of solid particles thermal energy storage unit. Appl Therm Eng 2006;26(5–6):513–8.

[17] Izquierdo-Barrientos MA, Sobrino C, Almendros-Ibáñez JA. Modeling and experiments of energy storage in a packed bed with PCM. Int J Multiph Flow 2016;86:1–9.

[18] Arkar C, Medved S. Influence of accuracy of thermal property data of a phase change material on the result of a numerical model of a packed bed latent heat storage with spheres. Thermochim Acta 2005;438(1–2):192–201.

[19] Bellan S, Gonzalez-Aguilar J, Romero M, Rahman MM, Goswami DY, Stefanakos EK, et al. Numerical analysis of charging and discharging performance of a thermal energy storage system with encapsulated phase change material. Appl Therm Eng 2014;71(1):481–500.

[20] Karthikeyan S, Velraj R. Numerical investigation of packed bed storage unit filled with PCM encapsulated spherical containers—a comparison between various mathematical models. Int J Therm Sci 2012;60:153–60.

[21] Bear J. Dynamics of fluids in porous media. New York: American Elsevier Publishing Company, Inc. 2013.

[22] Negrini AL, Fuelber A, Freire JT, Thoméo JC, Negrini AL. Fluid dynamics of air in a packed bed: velocity profiles and the continuum model assumption. Braz J Chem Eng 1999;16(4):421–32.

[23] Xia L, Zhang P, Wang RZ. Numerical heat transfer analysis of the packed bed latent heat storage system based on an effective packed bed model. Energy 2010;35(5):2022–32.

[24] Tabib MV, Johansen ST, Amini S. A 3D CFD-DEM methodology for simulating industrial scale packed bed chemical looping combustion reactors. Ind Eng Chem Res 2013;52(34):12041–58.

[25] Zhong W, Yu A, Liu X, Tong Z, Zhang H. DEM/CFD-DEM modelling of non-spherical particulate systems: theoretical developments and applications. Powder Technol 2016;302:108–52.
[26] Pakrouh R, Hosseini MJ, Ranjbar AA, Bahrampoury R. Thermodynamic analysis of a packed bed latent heat thermal storage system simulated by an effective packed bed model. Energy 2017;140:861–78.
[27] Boccardo G, Augier F, Haroun Y, Ferré D, Marchisio DL. Validation of a novel open-source work-flow for the simulation of packed-bed reactors. Chem Eng J 2015;279:809–20.
[28] Romero J, Soares JBP. A Monte Carlo method to quantify the effect of reactor residence time distribution on polyolefins made with heterogeneous catalysts: part II—packing density effects. Macromol React Eng 2018;12(4):1800002.
[29] Eppinger T, Seidler K, Kraume M. DEM-CFD simulations of fixed bed reactors with small tube to particle diameter ratios. Chem Eng J 2011;166(1):324–31.
[30] Dixon AG, Nijemeisland M, Stitt EH. Systematic mesh development for 3D CFD simulation of fixed beds: contact points study. Comput Chem Eng 2013;48:135–53.
[31] Argyropoulos CD, Markatos NC. Recent advances on the numerical modelling of turbulent flows. Appl Math Model 2015;39(2):693–732.
[32] Yakhot V, Smith LM. The renormalization group, the ε-expansion and derivation of turbulence models. J Sci Comput 1992;7(1):35–61.
[33] Kim Y, Hossain A, Nakamura Y. Numerical study of melting of a phase change material (PCM) enhanced by deformation of a liquid–gas interface. Int J Heat Mass Transfer 2013;63:101–12.
[34] Partopour B, Dixon AG. An integrated workflow for resolved-particle packed bed models with complex particle shapes. Powder Technol 2017;322:258–72.
[35] Mueller GE. Radial porosity in packed beds of spheres. Powder Technol 2010;203(3):626–33.